NUREG/CR-1787
LA-8547-MS

Experimental and Statistical Investigation of Thermally Induced Failure in Reactor Fuel Particles

University of California
LOS ALAMOS SCIENTIFIC LABORATORY
Post Office Box 1663 Los Alamos, New Mexico 87545

DISCLAIMER

NUREG/CR-1787
LA-8547-MS

R8

Experimental and Statistical Investigation of Thermally Induced Failure in Reactor Fuel Particles

J. L. Lunsford
R. J. Imprescia*
A. L. Bowman
C. E. Radosevich

NUREG/CR--1787

TI86 002689

Manuscript submitted: September 1980
Date published: October 1980

DISCLAIMER

NRC FIN No. A7014

*First Church of Religious Science, 1324 South Cheyenne, Tulsa, OK 74119.

UNITED STATES
DEPARTMENT OF ENERGY
CONTRACT W-7405-ENG. 36

EXPERIMENTAL AND STATISTICAL INVESTIGATION OF THERMALLY INDUCED FAILURE IN REACTOR FUEL PARTICLES

by

J. L. Lunsford, R. J. Imprescia, A. L. Bowman
and C. E. Radosevich

ABSTRACT

An incomplete experimental study into the failure statistics of fuel particles for the high-temperature gas-cooled reactor (HTGR) is described. Fuel particle failure was induced by thermal ramping from room temperature to temperatures in the vicinity of 2273 K to 2773 K in 2 to 30 h and detected by the appearance of ^{85}Kr in the helium carrier gas used to sweep the furnace. The concentration of krypton, a beta emitter, was detected by measuring the current that resulted when the helium sweep gas was passed through an ionization chamber.

TRISO fuel particles gave a krypton concentration profile as a function of time that built up in several minutes and decayed in a fraction of an hour. This profile, which was temperature independent, was similar to the impulse response of the ionization chamber, suggesting that the TRISO particles failed instantaneously and completely. BISO fuel particles gave a krypton concentration profile as a function of time that built up in a fraction of an hour and decayed in a fraction of a day. This profile was strongly temperature dependent, suggesting that krypton release was diffusion controlled, i.e., that the krypton was diffusing through a sound coat, or that the BISO coating failed but that the krypton was unable to escape the kernel without diffusion, or that a combination of pre- and postfailure diffusion accompanied partial or complete failure.

I. INTRODUCTION

The fuel particle heat-up experiment at the Los Alamos Scientific Laboratory was designed to contribute toward model development and verification for the LARC-1[1] code and to provide confirmation data for the General Atomic Company fuel failure model.

The development of fission product release codes such as LARC-1 has generated the need for fuel failure histories and fission product release constants. (See, in particular, the calculations described in the AYER,[2] SORS,[3] and the GASSAR-6[4] reports.) While the fuel failure models employed may differ according to application, they basically relate the failed fraction of fuel particles to the temperature as a parametric function of the irradiation history or age.

Fuel failure is a material process. The fuel failure model depends on results of experimental measurements on the properties of the fuel particle. In particular, it may include the interaction between the particle and the experimental environment, measured either explicitly or implicitly. Because a simple model is needed, the conditions under which the fuel failure histories are measured should be as close as possible to the accident conditions under which they are applied. Thus, the more the experiment differs from the environment in the reactor, the greater will be the interpretation required in the application of the fuel particle failure model to accident analysis. Unfortunately, it sometimes happens that fuel properties under transient conditions are not measured but are predicted analytically.[5]

Different pre- and postfailure fission product release mechanisms give rise to different pre- and postfailure release constants. These constants are used in the release codes to predict fission product migration and transport. The transition from the prefailure to the postfailure regime occurs with increasing time at temperature and with increasing radiation levels. To model the fission product transport process correctly, the failure statistics describing this transition must be well understood.

One of the more important and widely studied accident scenarios is the loss-of-forced circulation (LOFC) accident wherein the thermal response of the reactor is described by some generalized form of ramp function. In particular, the LARC series of codes addresses this specific accident trajectory. Consequently, the thermal ramp was employed as the experimental technique for testing fuel particle performance in the Los Alamos fuel particle heat-up experiments. In particular,

we used variations on a standardized ramp function with a 2273 K to 2773 K amplitude and a 2 to 30 h time base. Figure 1 indicates the shape of the ramp employed.

The experimental effort focused on the failure occurring in irradiated particles, or beads, supplied by the General Atomic Company. In the context of this work, failure is taken to be any loss of coating integrity induced by thermal ramping and detected by ^{85}Kr evolution. The failed fuel particles were not studied in detail. In this sense, the effort may be regarded as a study only of the statistics of failure and of the subsequent methodology of data treatment.

II. EQUIPMENT

The equipment used in the experiment was intended to induce coating failure by thermal ramping and to detect coating failure by monitoring the concentration of krypton in the furnace sweep gas. As the experiment progressed and our

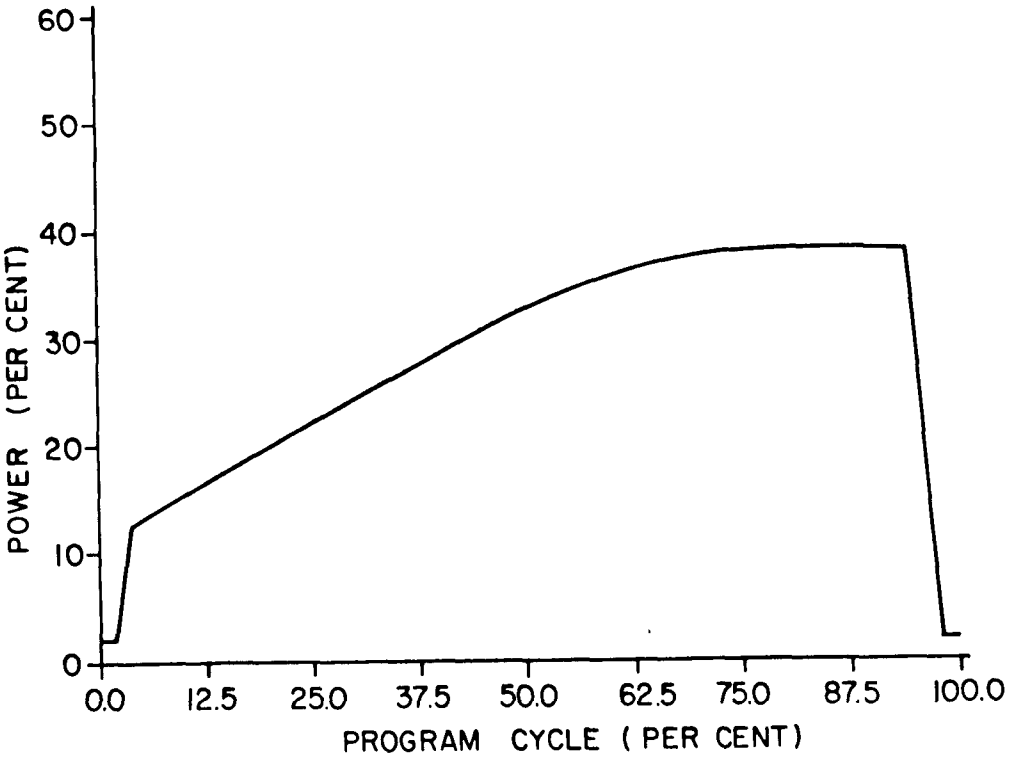

Fig. 1. Generalized ramp function used in the experiment. Maximum temperatures were varied from 2273 to 2773 K and the length of the time base was varied from 2 to 30 h.

experience with the equipment grew, certain changes were made in the equipmental configuration to solve evolving problems. Consequently, all of the data for the experiment could not be handled in the same way. However, no interpretation of results is attempted herein that is affected by differences in data treatment.

Figure 2 shows a schematic of the final experimental arrangement. The major components in the system were the high-temperature furnace and the ionization chamber. The furnace employs a liner tube of tantalum with a hot zone 10.5 by 180 mm long. The fuel particle was placed in a graphite boat in the center of the tantalum tube. Helium sweep gas was passed down this tube with a flow rate set by a high-performance controller. To minimize the reactivity of the helium gas with respect to the fuel particle, this helium was first purified in a titanium gettering furnace. When the fuel bead began to fail, the krypton within the coating was released into the sweep gas and carried out of the furnace through an ion trap into the ionization chamber. Because the krypton is a beta emitter, the current in the chamber was taken as a measure of the krypton concentration. However, any radioactivity in the ionization chamber will produce an ionization current. To minimize currents arising from sources other than krypton, the sweep gas was passed through a gettering furnace after exiting the high-temperature furnace and before entering the ionization chamber. In this way, only nonreactive gases could contribute to the ionization current. These commercial gettering furnaces operated at a temperature of 1123-1173 K with titanium wire charges. Purified helium from the inlet-side gettering furnace also was used to protect the internal components of the high-temperature furnace.

Those fuel particles containing thorium emitted radon during testing. Furthermore, at the higher temperatures, the precursors of radon escaped the fuel particle coating and contaminated the tantalum liner tube. This contamination tended to build with each successive fuel bead that was tested. The radon concentrations in equilibrium in the liner tube appeared to be quite large. Furthermore, because the radon is inert, it passed through the outlet-side gettering furnace and, because it is a beta emitter, gave rise to substantial currents in the ionization chamber. To reduce the magnitude of the interfering radon, we made use of the 55.6-s radon half-life. After the carrier gas exited the liner tube, we passed it through 15.24 m of 1/4 in. copper tubing, through the exit-side gettering furnace, and through another 30.48 m of copper tubing. This tubing represents 836 cc of volume. If plug flow were assumed, then a helium flow rate of 1 cc/s will have caused the radon gas to be separated from its precursors by

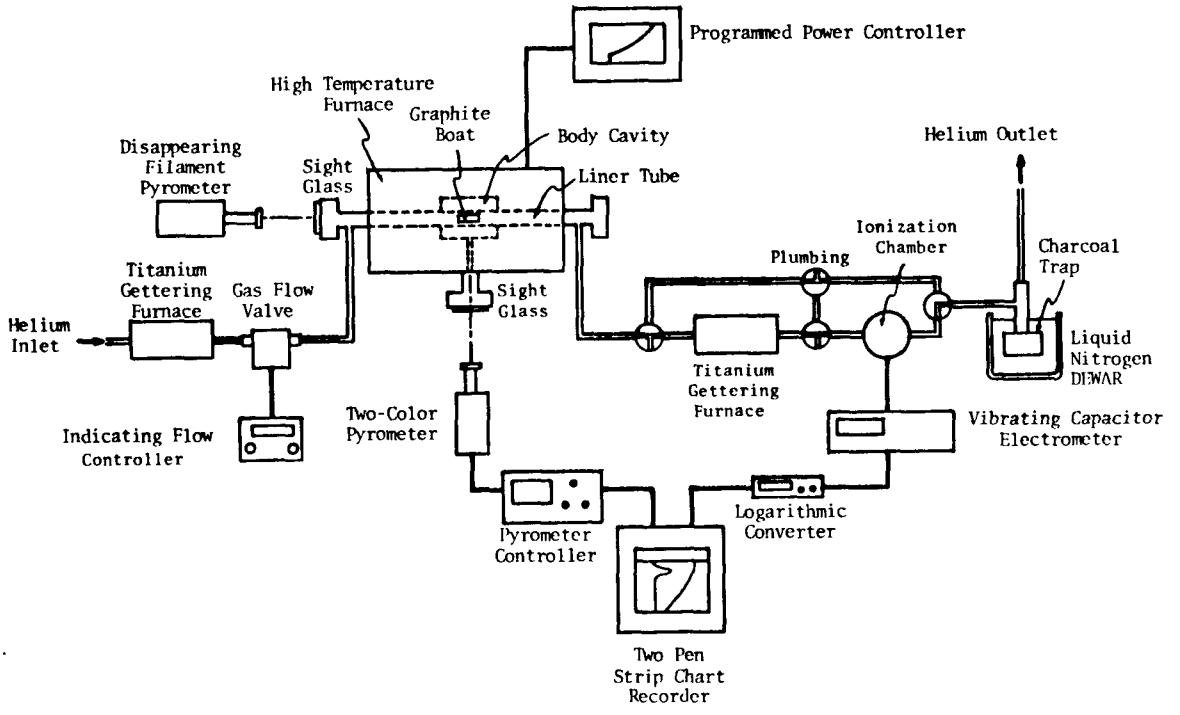

Fig. 2. Experimental configuration. The principal components in the experiment were the high-temperature furnace and the ionization chamber.

just over 15 half-lives. Consequently, the concentration of radon in the helium sweep gas will have decayed by a predicted factor of 33 000. Independent tests have indicated that the plug flow assumption is correct to about 15%. In other words, the 45.72 m of copper tubing in the line reduced the radon interference by a factor of some 30 000. In this way, interfering radon levels that produced peak backgrounds as high as 5 000 fA were finally reduced to the order of 1 fA. This was important, as the true krypton signal for the BISO particles -- when recovered from the noise level -- peaked at less than 100 fA.

The boat temperature could be determined by an optical pyrometer sighting down the axis of the tube. However, the length-to-diameter ratio of the liner tube and the creep of the liner tube in service made it impossible to obtain direct measurement of the boat temperature by continuous, automatic recording techniques. Instead, it was necessary to determine the boat temperature indirectly. The high-temperature furnace used in this experiment has a cavity in the center that measures 56 by 180 mm long. The temperature of the liner tube, which extends through this cavity, equilibrates with the cavity temperature by radiant energy transfer. The temperature of the boat within the liner tube was measured by a disappearing filament pyrometer that sighted down the axis of the furnace

liner tube. The temperature of the cavity was measured by a two-color pyrometer aligned into the cavity through a sight glass on the centerline of the furnace body. (This pyrometer has a continuous temperature range from 1 273 K to 3 273 K and automatically recalibrates itself every 15 min.)

During an experimental run, the boat temperature was measured periodically. The cavity temperature was recorded continuously. For each run, a nonlinear least-squares fit was made to the boat temperature as a function of the power delivered to the furnace. This allowed us to treat time-temperature profiles analytically and thereby to derive some of the statistical results to be presented later in this paper.

Fission product release occurs with increasing temperature before and after fuel particle failure. The chemically active period of the heating ramp is restricted to a few hours. Consequently, for release from a single particle to become significant in such a short time, the release rates must be large and the temperatures must be high. At such temperatures, most species that escape will be gaseous. For these gases, the helium sweep gas carried the fission products away from the fuel bead. As the sweep gas moved along the liner tube, the gas temperature dropped and condensible species plated out. The inert gases were swept along without interaction, but with some distortion of the concentration profiles along the tube. By monitoring the beta activity in the ionization chamber, it was possible to gain information about the condition of the particle coating.

We also carried out trapping experiments on the carrier gas using activated charcoal at liquid nitrogen temperatures. As anticipated, the trapped species gave rise to concentration levelsin the trapping canister that were below detection as measured with state-of-the-art mass spectrometric techniques.

III. EXPERIMENTAL RESULTS

Six types of fuel particles were present in the beads received from the General Atomic Company. Table I summarizes fuel particle histories in the shipment. Table II summarizes the test results. During the course of the work, some 66 experiments were conducted. Some of these experiments were thermal runs made without a fuel particle in the furnace, some were room-temperature experiments with fuel particles broken with a piston device in situ in the furnace liner, while most were thermal runs made with a fuel particle in place in the

TABLE I

FUEL PARTICLE IRRADIATION HISTORIES

Capsule	Coating	Kernel	Temp. (K)	Irradiation Fast Fluence 10^{21} n/cm^2	Conditions Kernel Burnup (% FIMA)
HB-5	TRISO	$U(C_{3.0}O_{0.5}$	973.15	4.9	59.0
FTE-14	TRISO	UC_2	1 273.15	1.2	23.0
F-30	TRISO	(Th/U)C	1 524.15	9.1	18.2
P13R	BISO	ThO_2	1 273.15	11.4	4.4
P13S	BISO	ThO_2	1 213.15	11.6	4.1
HT-28	BISO	ThO_2	1 173.15	6.4	7.2

furnace. In most cases, thermal runs to temperatures above 2 473 K caused bead failure as detected by the appearance of ^{85}Kr in the ionization chamber.

In actual testing, the question arises as to whether the appearance of an ionization current peak indicates instantaneous and catastrophic failure of a

TABLE II

FUEL PARTICLE TESTING RESULTS

Capsule	Total Number Received	Number Tested at Room Temperature	Number Tested at Elevated Temperature	Total Number Tested
HB-5	30	0	1	1
FTE-14	50	6	2	8
F-30	50	0	31	31
P13R	20	3	13	16
P13S	20	0	1	1
HT28	10	0	0	0
Totals	180	9	48	57

fuel particle. The way the krypton escapes the particle and travels to the ionization chamber through the outlet gettering furnace and the associated plumbing determines what interpretation will be placed on the shape of the current trace. It is instructive, therefore, to examine the simplest possible case: namely, the current peak resulting from a mechanical crushing at room temperature of a fuel particle located in the center of the furnace. This was accomplished with a small piston device that was designed to crush and grind a single fuel particle. The mechanical breaker, which was hand operated, could be inserted through a vacuum seal in-line with the furnace liner tube. To operate the breaker, a fuel particle was placed in the chamber, the device was inserted into the furnace, helium flow was established with both the inlet and outlet gettering furnaces operating, and the bead was broken in situ. Figure 3 (Run No. 58) shows the resultant current trace for a TRISO particle. The dotted line represents the beginning of the current peak as determined by monitoring the most sensitive scale of the electrometer voltmeter. The time delay (TD) for the appearance of the krypton in the ionization chamber was measured at 11.8 min for the case of a TRISO/FTE-14 break with 45.72 m of copper tubing and a flow rate of 1 cc/s through a 250-cc ion trap into a 1 000-cc ionization chamber. For the curve in question, the rise time (RT) is 0.38 ks; the width at half maximum (WAHM) is 0.93 ks. For a BISO particle, Fig. 4 (Run No. 63) indicates the response of the ionization current for a mechanical P13R break with 45.72 m of copper tubing and a flow rate of 1 cc/s through a 250-cc ion trap into a 1 000-cc ionization chamber. This trace exhibits a TD of 11.8 min, a RT of 0.41 ks, and a WAHM of 1.05 ks. Because the current levels for the BISO are reduced an order of magnitude from those for the TRISO, these data suggest that a large reduction of the krypton concentration leaves the TD unchanged and increases the WAHM and the RT by only a per cent or so.

It was desirable to determine quantitatively the relative current output of the various particle types. The area under the current curve as a function of time proves to be deceptive, as both a low seep rate and a large ionization volume will result in larger values for the integral. Consequently, a normalized area was calculated as

$$A_n = \frac{f}{v} \int I(t)\, dt \ , \qquad (1)$$

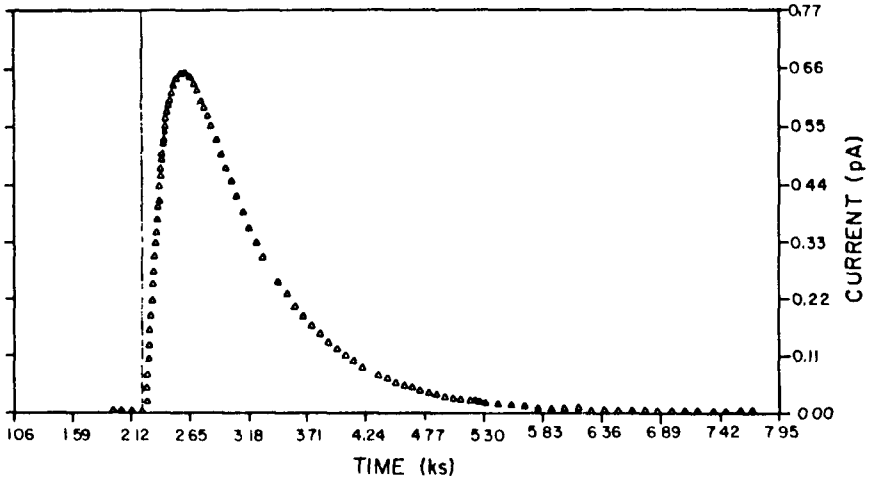

Fig. 3. Room-temperature break of a TRISO/FTE-14 fuel particle with 45.72 m of tubing and 1-cc/s sweep rate through a 250-cc ion trap into a 1 000-cc ionization chamber. Note the current peak of 0.652 pA. Integrated area under the peak is 7.36E-01 pA. (Run No. 58.)

where f is the sweep rate in cc/s, v is the volume of the ionization chamber in cc, and the area A_n is in pA. (The calculation was adjusted for background.) The TRISO/FTE-14 trace peaks at 0.652 pA, with an integrated area of 7.36E-01 pA. The BISO/P13R peaks at 0.075 4 pA, with an integrated area of 8.72E-02 pA. This puts the integrated krypton activity escaping the room-temperature TRISO break at 8.4 times that for the BISO.

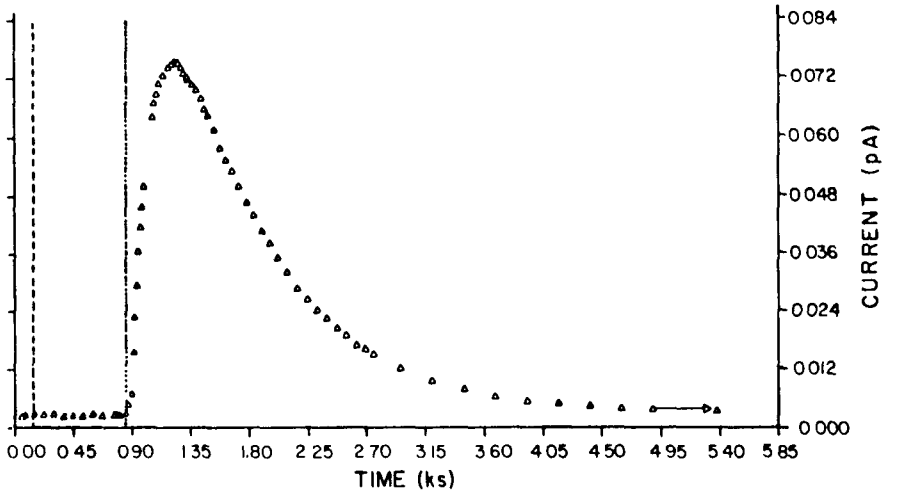

Fig. 4. Room-temperature break of a BISO/P13R fuel particle with 45.72 m of tubing and a 1-cc/s sweep rate through a 250-cc ion trap into a 1 000-cc ionization chamber. Note the current peak of 0.075 4 pA. Integrated area under the peak is 8.72E-02 pA. (Run No. 63.)

Thermal failure in TRISO fuel particles was accompanied by a current trace having much the same appearance as for the mechanical break at room temperature. Figure 5 (Run No. 53) shows the current trace for a TRISO/F-30 bead. (The tantalum liner tube breached during the run and the gas flow was adjusted twice to compensate for bypass leakage. The times corresponding to these two adjustments are indicated by the vertical dashed lines. The solid line indicates the start of the power ramp down.) The current trace peaks at 0.748 pA, with a WAHM of 2.97 ks and a normalized area of 1.209 pA. This width is 3.2 times larger than the WAHM for the room-temperature break, and the area is 1.9 times larger. While the parameters associated with the run at temperature are larger than those for the room-temperature break, the conditions differed when the data were taken. The room-temperature break was carried out with 45.72 m of tubing and a 1-cc/s sweep rate through a 250-cc ion trap into a 1 000-cc ionization chamber. The break at temperature occurred in a test with 15.24 m of tubing and a 0.5-cc/s flow rate through a 250-cc ion trap into a 1 000-cc ionization chamber. Furthermore, the thermally induced turbulence in the liner tube at 2 773 K is appreciable. Nevertheless, the appearance of the curve tends toward that of the mechanical break at room temperature. More important is the fact that the power ramp down at 12 ks did not perturb the krypton release curve. Finally, the tail of the current trace in Fig. 5 reflects a residual background caused by the run,

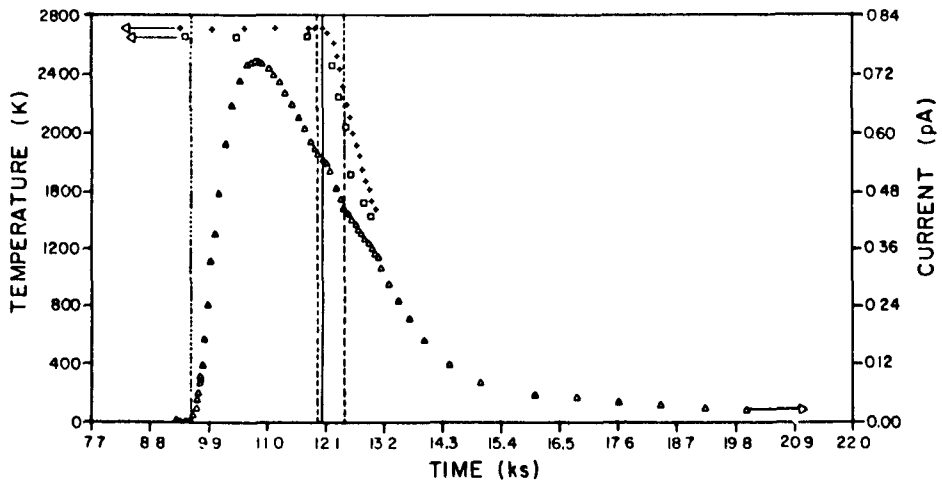

Fig. 5. Thermal break of a TRISO/F-30 fuel particle with 15.24 m of tubing and a 0.5-cc/s sweep rate through a 250-cc ion trap into a 1 000-cc ionization chamber. Squares indicate boat temperatures; crosses indicate cavity temperatures. Note the current peak of 0.748 pA. Integrated area under the peak is 1.209 pA. (Run No. 53.)

indicating some contamination. On balance, although the parameters characterizing the current traces for the two runs are distinctly different, so are the conditions under which they were measured. As the experimental techniques were changing drastically during this phase of the work, we favor an interpretation that the TRISO particles were failing instantaneously.

Thermal failure in BISO fuel particles was accompanied by a current trace having a totally different appearance from the mechanical break at room temperature. Figure 6 (Run No. 66) shows the current trace for a BISO/P13R bead. (The curve has clearly been interrupted by the power ramp down after more than 6 h into the run and 4 h at temperature. The vertical chain-dotted lines indicate changes in the power program.) The current trace peaks at 0.085 8 pA with a WAHM greater than 14.0 ks and a normalized area of 1.15 pA. This width is 13.3 times larger than the WAHM for the room-temperature break and the area is 13.2 times larger. Both runs were conducted with 45.72 m of tubing and a sweep rate of 1 cc/s through a 250-cc ion trap into a 1 000-cc ionization chamber. Both the numerical parameters and the appearance are totally different. More importantly, the shape of the curve clearly implies that the release of krypton is diffusion-controlled as a temperature drop of 260 K at 21 ks caused decrease in the krypton release rate of a factor of 6.3, and a subsequent drop of 180 K at 26 ks caused a drop in the release rate by a factor of 5.3. Consequently, we favor an interpretation that the BISO fuel particles were not failing instantaneously, but were losing krypton by diffusion through a sound coating.

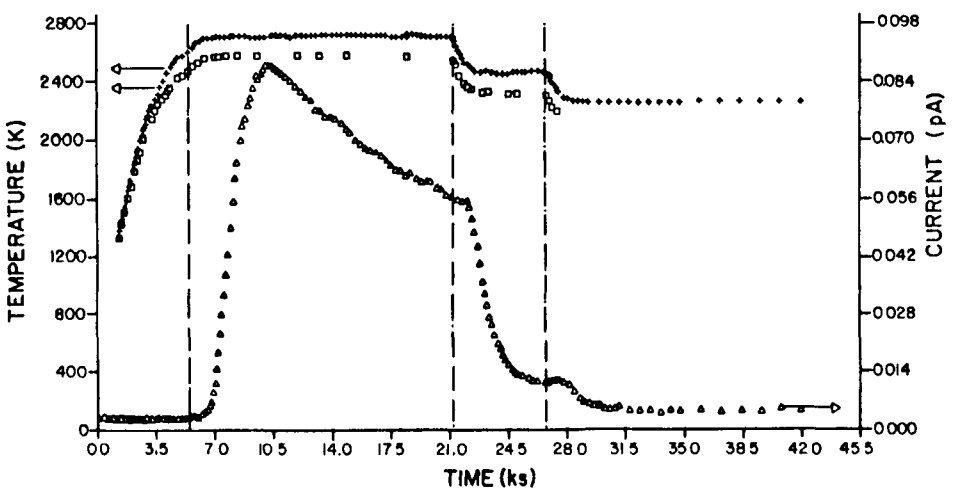

Fig. 6. Thermal break of a BISO/P13R fuel particle with 45.72 m of tubing and a 1-cc/s sweep rate through a 250-cc ion trap into a 1 000-cc ionization chamber. Squares indicate boat temperatures; crosses indicate cavity temperatures. Note the current peak of 0.085 pA. Integrated area under the peak is 1.159 pA. (Run No. 66.)

IV. STATISTICAL RESULTS

As indicated in Table II, the test results for the TRISO bead are most numerous for the F-30 fuel particle. For the 31 F-30 particles tested at temperature, 5 were tested with background levels of sufficient magnitude as to render interpretation impossible. For the remaining 26 runs, the data are consistent with the interpretation of instantaneous failure as depicted in Fig. 5. Before and after failure, different release mechanisms will give rise to different release constants. To quantify the transition from prefailure to postfailure mechanisms, we chose to examine an Arrhenius rate expression of the form

$$e^{-\frac{Q}{RT}} , \tag{2}$$

where Q is an activation energy in joules, R is the universal gas constant in joules per mole degree K, and T is the absolute temperature in degrees K. If thermal damage is assumed to be exponentially related to temperature, and if damage limit is independent of temperature, then the integral of Eq. (2) becomes a criterion for transition from prefailure to postfailure release mechanisms. Thus, we are interested in the statistical distribution of the quantities

$$x_n = \int_0^{t_o} e^{-\frac{Q}{RT}} dt \quad , \quad n = 1 \ldots, N , \tag{3}$$

where the integral is evaluated from zero to the time of failure t_o for the bead under test for each of the N thermal runs. When the number of beads tested becomes sufficiently large, the repeated evaluation of Eq. (3) for successive tests generates a density function f(x). The quantity of interest to the code developer is the fraction of fuel particles surviving. Denoting this distribution as F, we have

$$F(x) = 1 - \int_0^x f(x') \, dx' \quad . \tag{4}$$

In this sense, F(x) is the complement of the cumulative distribution of the density function f(x).

To calculate F(x), it is necessary to evaluate Eq. (3). This, in turn, will require the determination of $T_n(t)$, the temperature history of each bead n as a function of time throughout the test. The data were fitted to a nonlinear impulse model. Figure 7 (Run No. 10) shows a fit to a thermal run with a TRISO fuel particle. The chain-dotted line indicates where the power program was halted and the power set point was manually increased. The dashed line represents the time of fuel particle failure, and the solid line represents the initiation of the power ramp down.

To calculate the survival distribution F(x), a value must be assigned to the activation energy Q in Eq. (3). In isothermal testing, a value of activation energy could be revealed by plotting the logarithm of a function of the rate against the reciprocal of the absolute temperature. As the testing carried out in this work was nonisothermal, no such procedure is available. Instead, it was decided to use that value of activation energy Q that would minimize some statistical property of the distribution F(x).

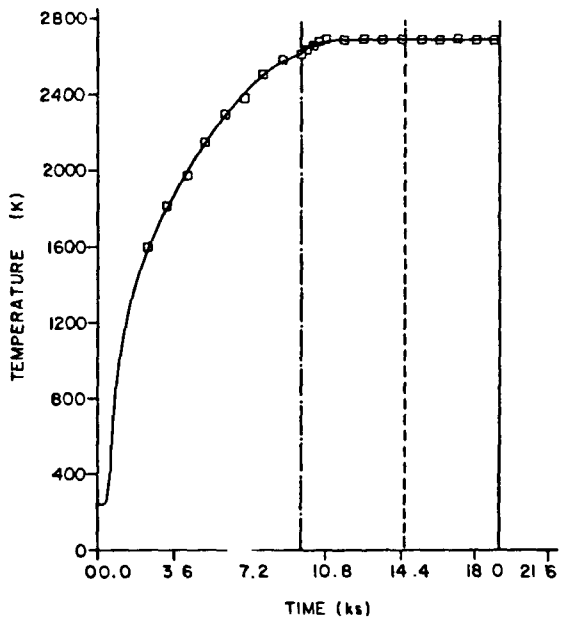

Fig. 7. Nonlinear least-squares fit to the temperature data of Run No. 10. The vertical chain-dotted line at 9.6 ks indicates where the programmer was turned off and the power set point was increased manually.

For any distribution, the mean is defined

$$\mu = \frac{1}{N} \sum_{n=1}^{N} x_n \quad , \tag{5}$$

the variance is defined

$$\gamma = \frac{1}{N} \sum_{n=1}^{N} (x - \mu)^2 \quad , \tag{6}$$

and the coefficient of dispersion is the ratio

$$r = \frac{\mu}{\sigma} \quad , \tag{7}$$

where σ is the standard deviation

$$\sigma = \sqrt{\gamma} \quad . \tag{8}$$

Figure 8 contains a plot of the coefficient of dispersion as a function of the activation energy Q as a chain-dashed line. Here, Q is varied from zero to 1 600 kJ. The values near zero are clearly nonphysical and generate a limb of the curve that is of no interest. The plot indicates a minimum in the coefficient of dispersion around 825 kJ. However, the minimum is extremely broad, indicating that the goodness of fit is relatively insensitive to the activation energy Q.

To calculate F(x) from Eq. (4), f(x) must be approximated in some way. We elected to fit the densitv function f(x) to the incomplete gamma function. This distribution is of the form

$$\gamma(x) = \frac{x^{(\alpha - 1)} e^{-x/\beta}}{\beta^{\alpha} \Gamma(\alpha)} \quad , \tag{9}$$

where the α and β are the two disposable constants for the gamma distribution with zero origin. The form is extremely general, taking on a wide variety of

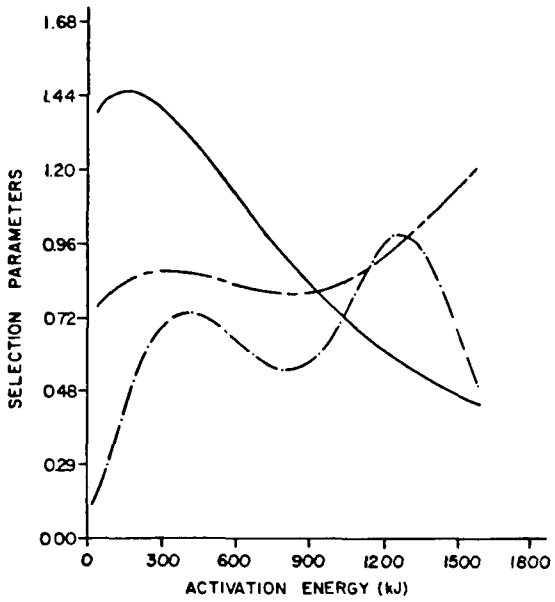

Fig. 8. Plot of the coefficient of dispersion (chain-dashed line), the α of the incomplete gamma function (solid line), and the significance level of the composite hypothesis (chain-dotted line) against the activation energy Q. The coefficient of dispersion goes through a minimum around 825 kJ: the α of the incomplete gamma function is 1.0 at about 722 kJ.

shapes as determined by the constants α and β. When $\alpha = 1$, the distribution reduces to the exponential distribution

$$e(x) = \frac{1}{\beta} e^{-x/\beta} , \qquad (10)$$

where the β of Eq. (10) is the β of Eq. (9).

The calculation of the parameters of the incomplete gamma function was carried out using a method of maximum likelihood estimators.[6] The β of Eq. (9) is a scale factor and is uninteresting in the context of the present discussion. The parameter α calculated as indicated above is plotted in Fig. 8 as the solid line. It is interesting to note that the value of α is close to one over the range of the minimum in the coefficient of dispersion. When α is close to one, the resultant distribution is close to exponential. The exponential distribution is highly desirable because of its nearly ideal properties in statistical problems. Consequently, it was considered interesting to calculate a test for the goodness of fit of the data to an exponential distribution. This was done using a method outlined elsewhere[7] and the significance level of the composite hypothesis

is plotted in Fig. 8 as a chain-dotted line. (The composite hypothesis is the postulate that the density function tested has zero origin and an exponential distribution. The significance level tests the null hypothesis: namely, that the composite hypothesis is an acceptable presupposition. A significance level below 0.1 would be said not to support the composite hypothesis.) Because the plot of the significance for the test for exponentiality is in excess of 0.5 over the entire range of Q, it was deemed acceptable to represent the data as an exponential distribution by selecting a value of activation energy Q for which the α of Eq. (9) is one. This corresponds to an activation energy of 722 kJ.

The density function f(x) for an activation energy Q of 722 kJ is listed in Table III. The survival distribution F(x) for this density function is plotted in Fig. 9. Also plotted is the exponential fit to the data with a value for β of 2.82E-11. The entire test program for the F-30 fuel particle is thereby reduced to two constants.

The calculation of the survival fraction for the TRISO/F-30 fuel particle becomes quite simple. For a differential region, the fraction of particles in the pre- and postfailure regimes may be calculated by first calculating the reaction coordinate

$$x = \int_0^{t_o} e^{-\frac{Q}{RT}} dt \qquad (11)$$

TABLE III
DISTRIBUTION OF THE REACTION COORDINATE

Column 1	Column 2	Column 3	Column 4	Column 5
0.011 42	1.051 05	1.576 92	3.132 26	4.286 75
0.029 07	1.212 70	1.831 39	3.312 86	4.343 72
0.319 92	1.301 29	1.900 70	3.773 15	4.898 64
0.654 85	1.342 96	2.308 35	3.936 56	5.519 51
0.798 27	1.479 95	2.897 06	4.101 62	8.086 16
				9.308 71

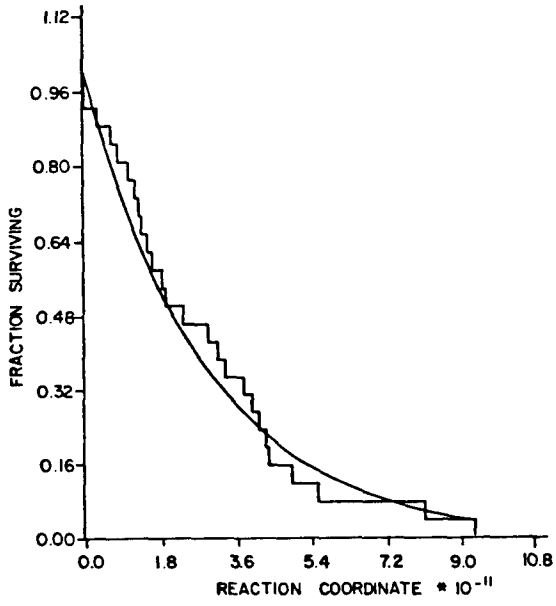

Fig. 9. Survival statistics for the TRISO/F-30 test data. The stepped line is the plot of the experimental data with an assumed activation energy of 722 kJ. The smooth line is the exponential fit to the experimental data for a β value of 2.82E-11.

and then calculating the fraction surviving as

$$F(x) = e^{-\frac{x}{\beta}} , \tag{12}$$

where the activation energy Q is 722 kJ, the exponential constant β is 2.82E-11, and the integral of Eq. (11) is carried out over the time-temperature profile T(t) for the region in question.

The derivation of the survival distribution F(x) proceeded from physical assumptions regarding an Arrhenius rate function with a single activation energy and a damage limit for the individual fuel particle, both independent of temperature. If such assumptions are correct, they will make the resultant model more physical. However, the accuracy of the final fit as carried out here is unaffected by the correctness of these presumptions. In this sense, a physically correct model may be superior under conditions of extrapolation, but will give equivalent answers under interpolation. In other words, the validity of the data representation given here does not depend in any way upon the validity of the physical model to which the data were fitted.

V. COMPARISON WITH THE ANALYTIC FUEL FAILURE MODEL

A comparison was made between the experimental results of this study and the analytic fuel failure model used in the other studies cited in this report. For this purpose, the accident trajectory following the loss of forced cooling was selected as the computational medium.

The analytic fuel failure model, which is independent of time, is given by the relations

$$F(T) = 1.0 \quad , \quad T < T_1 \quad , \tag{13}$$

$$F(T) = c_0 + c_1 T \quad , \quad T_1 < T < T_2 \quad , \tag{14}$$

and

$$F(T) = 0.0 \quad , \quad T > T_2 \quad , \tag{15}$$

where T is the maximum temperature that the fuel particles have experienced and the constants c_0 and c_1 are selected to scale the distribution linearly between 1 and 0 as a function of the temperatures T_1 and T_2, respectively. The temperatures used in the comparison calculation were taken for fuel material less than 12 years old; namely,

$$T_1 = 1\ 858.15 \text{ K} \tag{16}$$

and

$$T_2 = 1\ 998.15 \text{ K} \quad . \tag{17}$$

The core temperature profile for the LOFC accident is tabulated in the LARC-1 report for the first 20 h after the initiation of the accident.[1] This distribution was used to calculate LOFC survival distributions for both the experimental and analytical models. The results of the calculations are plotted in Fig. 10. The solid line represents the results of the calculation using the analytical model of Eqs. (13-17). The dashed line is the same calculation with the fuel failure model of Eqs. (11-12). The fuel particle population as

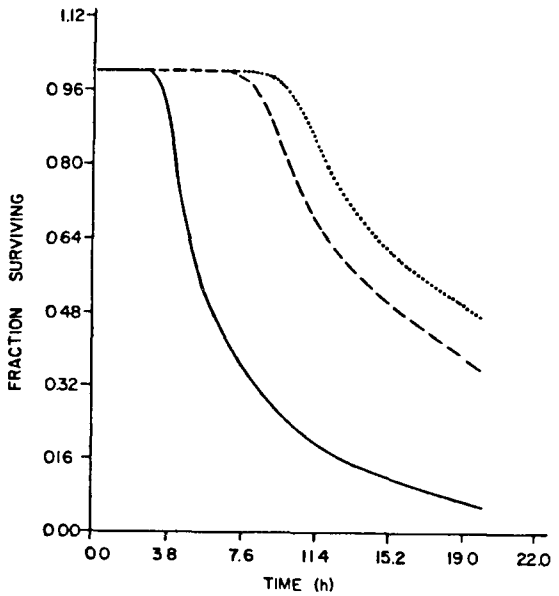

Fig. 10. Fuel particle survival distributions for analytical (solid line), experimental (dashed line), and hypothetical (dotted line) fuel particle failure models during the accident trajectory for an LOFC accident.

calculated with the experimental model is seen to remain intact for some 4 h longer than is the case for the analytical model. The dotted line represents a hypothetical fuel failure model with a statistical distribution identical to that for the F-30, but with a temperature characteristic raised some 200 K, indicating that an increase in thermal resistance has postponed the onset of fuel particle failure by some 2 h in the LOFC accident trajectory. This suggests a rule of thumb: relative to the F-30 Ft. St. Vrain prototypical fuel performance in an LOFC accident, an increase in the thermal resistance of 100 K will result in a 1-h increase in the onset of fuel failure.

The use of the analytical model definitely constitutes a conservative estimate of fuel particle behavior. This is indicated in Fig. 10 and again in Fig. 11, where the rate of fuel failure is plotted for the two fuel particle models. The peak for the experimental model is delayed, reduced in amplitude, and broadened relative to the analytical model, all by a factor of 2.5. The plot of the failure rate of the hypothetical fuel particle (dotted line) suggests that enhanced resistance to thermal failure will markedly reduce peak failure rates.

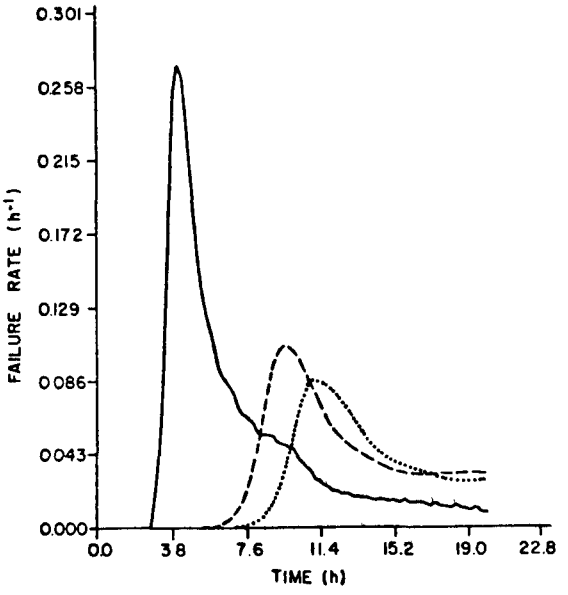

Fig. 11. Fuel particle failure rates for analytical (solid line), experimental (dashed line), and hypothetical (dotted line) fuel particle failure models during the accident trajectory for an LOFC accident.

ACKNOWLEDGMENTS

The authors would like to acknowledge the many useful conversations concerning the direction of the work with C. E. Apperson, Jr., J. E. Foley, and the helpful discussions on statistics with R. J. Beckman.

REFERENCES

1. L. M. Carruthers and C. E. Lee, "LARC-1: A Los Alamos Release Calculation Program for Fission Product Transport in HTGRs During the LOFC Accident," Los Alamos Scientific Laboratory report LA-NUREG-6563-MS (November 1976).

2. R. G. Lawton, "The AYER Heat Conduction Computer Program," Los Alamos Scientific Laboratory report LA-5613-MS (May 1974).

3. M. H. Schwartz, D. B. Sedgley, and M. M. Mendonca, "SORS: Computer Programs for Analyzing Fission Product Release from HTGR Cores During Transient Temperature Excursions," General Atomic Company report GA-A12462 (April 1974).

4. GASSAR-6, General Atomic Standard Safety Analysis report, GA-A13200 (July 1975).

5. C. L. Smith, "Fuel Particle Behavior Under Normal and Transient Conditions," General Atomic Company report GA-A12971 (GA-LTR-15)(October 1974).

6. N. L. Johnson and S. Kotz, Continuous Univariate Distributions-1 (Houghton Mifflin Co., New York, 1970) pp. 160-190.

7. S. S. Shapiro and M. B. Wilk, "An Analysis of Variance Test for the Exponential Distribution (Complete Samples)," Technometrics 14, 2 (May 1972).

DISTRIBUTION

	Copies
Nuclear Regulatory Commission, R8, Bethesda, Maryland	298
Technical Information Center, Oak Ridge, Tennessee	2
Los Alamos Scientific Laboratory, Los Alamos, New Mexico	50
	350

DO NOT MICROFILM
COVER

Available from

GPO Sales Program
Division of Technical Information and Document Control
US Nuclear Regulatory Commission
Washington, DC 20555

and

National Technical Information Service
Springfield, VA 22161